Bionanocomposites for Magnetic Removal of Water Pollutants

F.L. Sousa, A.L. Daniel-da-Silva, N.J.O. Silva and T. Trindade

Abstract Magnetic separation in water remediation processes is of great interest in current environmental technologies. An important aspect in this field has been the development of efficient sorbents for water purification units, namely by exploiting other functionalities that might originate more sustainable technologies. This chapter describes the state-of-art on the chemical preparation of magnetic sorbents comprising inorganic particles and biopolymer matrices. Fundamental aspects related to nanoparticle synthesis of iron oxides and nanomagnetism will be first addressed. The use of these particles in biopolymers matrices such as polysaccharides will be then reviewed as an innovative strategy aiming at production of eco-friendly sorbents for magnetic separation.

Keywords Biopolymers · Magnetic nanoparticles · Bionanocomposites · Magnetic separation

1 Introduction

Water is the most essential resource for life. The population growth and fast development of industrialization and intensive agricultural activities has increased the demand for treated water. Contamination of surface and ground waters by effluent discharges has become a critical environmental issue and attracted global concern over the past years [3, 71, 96]. Heavy metal ions, dyes, phosphates and nitrates, radioactive species, and pharmaceuticals are examples of water contaminants [3]. These contaminants can compromise the integrity of ecological cycles and have an impact on human health through drinking water and by integration in the food

F.L. Sousa · A.L. Daniel-da-Silva · T. Trindade (✉)
Department of Chemistry and CICECO, University of Aveiro, 3810–193 Aveiro, Portugal
e-mail: tito@ua.pt

N.J.O. Silva
Department of Physics and CICECO, University of Aveiro, 3810–193 Aveiro, Portugal

V.K. Thakur and M.K. Thakur (eds.), *Eco-friendly Polymer Nanocomposites*,
Advanced Structured Materials 74, DOI 10.1007/978-81-322-2473-0_9

chain, causing serious health and environmental effects, which may include carcinogenicity, reproductive impairment, developmental and immune system changes, and endocrine disruption [3, 91].

Consequently, water treatment has been a subject of paramount importance that nowadays requires more sustainable technologies. In order to provide long-term high quality water or to enable water recycling, there has been research in alternative remediation processes, for example, involving chemically modified nanometer sized adsorbents, ion exchangers, or systems that can also be of interest for bioapplications [3, 71, 96]. Various materials have been used for these purposes such as activated carbon, clays, siliceous materials, zeolites, and biopolymers [1, 9, 32, 74, 92] among others. However, in some cases the applications have been limited by the associated costs, regeneration, and limited cycles of application, among other factors. Alternatively, the use of low-cost and eco-friendly sorbents composed of natural polymers has gained significant interest over the recent years owing to their unique intrinsic properties such as biodegradability, easy availability, flexibility, easy processing, and impressive physico-mechanical properties [92-88]. These biopolymers are renewable materials, environmentally friendly, generally nontoxic, biodegradable, and combine excellent functional properties [24]. The combination of magnetic nanoparticles (MNPs) and biopolymers can lead to bionanocomposites responsive to external magnetic stimuli [17]. Although magnetic properties have been extensively exploited in magnetically driven drug transport for target delivery, they can also be relevant for magnetic separation of water pollutants [96, 18, 67]. Other properties of magnetic bionanocomposites are equally important for their successful application as sorbents in water treatment. Among these, specific surface area, particle size, pore diameter, morphology, and chemical surface functionalization are particularly relevant [71]. High adsorption capacities are associated to sorbents with effective high specific surface areas and the required functional groups for interaction with target contaminants [3].

This chapter provides an overview of the literature disclosed in the past decade in the field of magnetic biocomposites for water treatment applications. Emphasis is given to the most common methodologies for preparation of magnetic composites of polysaccharides and to studies devoted to the above-mentioned applications. Some general concepts on the magnetic properties of magnetic nanoparticles (MNPs) are summarized, considering the specific properties required for magnetic separation.

2 Magnetic Polysaccharide Composites

A magnetic bionanocomposite is defined here as a material comprising magnetic nanoparticles dispersed in a biopolymer matrix. The performance of such materials in the context of sustainable nanotechnologies has attracted global interest in recent

Table 1 Polysaccharides commonly used in the preparation of bionanocomposites

Polymer	Source	Ionic character	Functional groups
Agarose	Marine red algae	Neutral	OH
Alginate	Brown algae	Anionic	OH, COO^-
Carrageenan	Red seaweeds	Anionic	OH, OSO_3^-
Chitosan	Shelfish and fungi cell wall	Cationic	OH, NH_3^+
Dextran	Produced by lactic acid bacteria	Neutral	OH
Gum arabic	Acacia tree	Anionic	OH, COO^-
Gum kondagogu	Cochlospermum gossypium tree	Anionic	OH, COO^-
Starch	Green plants	Neutral	OH

years, leading to extensive research into their synthesis and subsequent applications. In particular, polysaccharides have been commonly used for coating MNPs, including chitosan, dextran, alginate, agarose, carrageenan, gum Arabic, cellulose derivatives, and starch. Table 1 lists polysaccharides commonly used to prepare magnetic biocomposites in the context of environmental applications and the respective structural formulae are shown in Fig. 1. Nanoparticles coated with such biopolymers generally possess high adsorption capacities, rapid adsorption rates, even when present in low amounts and at short equilibrium times, and in certain conditions can be reusable [24].

2.1 Preparation Techniques of Magnetic Bionanocomposites

Herein we draw our attention to preparative routes for production of magnetic bionanocomposites composed of biopolymers and magnetic nanoparticles. This section starts to outline some chemical methods of iron oxide MNPs that are often used as fillers in composite materials envisaging water treatment procedures. The preparative routes for magnetic bionanocomposites are then reviewed, by distinguishing preparative methods that are based in blends of the components from those in which the MNPs are produced in situ.

2.1.1 Inorganic Nanoparticles

Among the most used MNPs, magnetite (Fe_3O_4) and maghemite (γ-Fe_2O_3) have sparked great interest in water treatment research [96, 39, 84]. These iron oxides show biocompatibility, low toxicity, size tuned magnetic behavior, and possibility to up-scale synthesis [71, 18, 36]. Several synthetic methods are available for preparation of iron oxide nanoparticles with appropriate size and distribution, these include: co-precipitation of Fe(II) and Fe(III) salts, hydrolysis and thermolysis of iron containing precursors, chemical reactions in microemulsions, hydrothermal

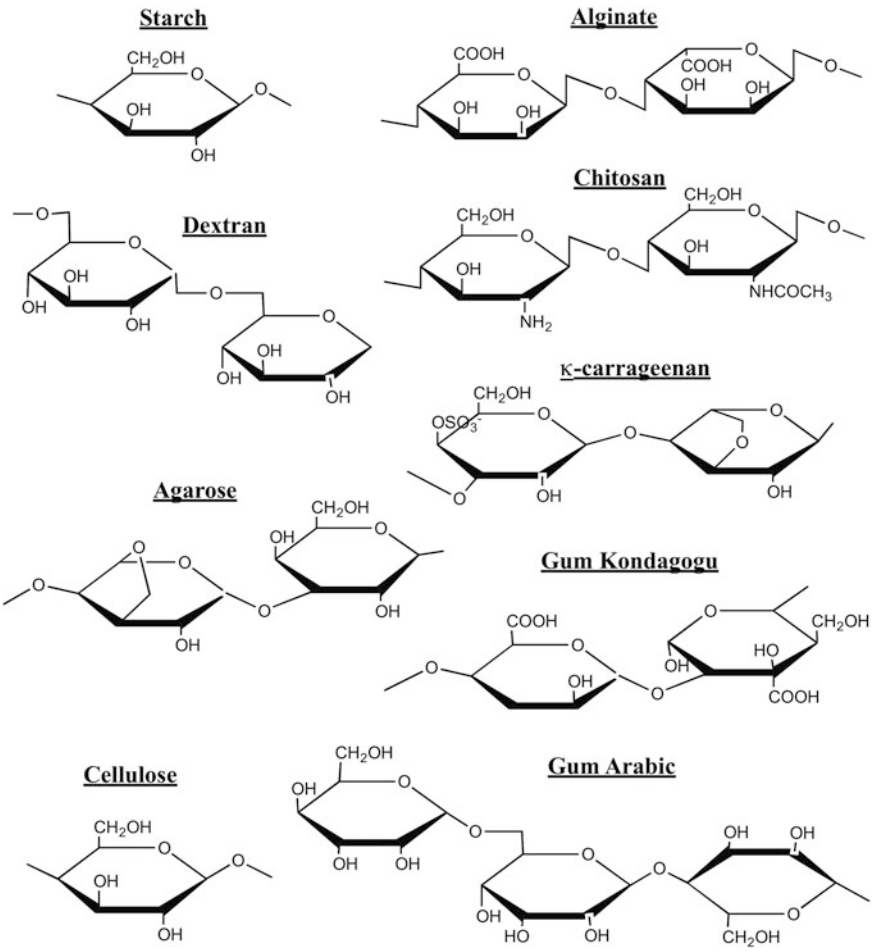

Fig. 1 Structural formulae of common polysaccharides

synthesis, sonochemical reactions [20, 43, 48]. By reaction of Fe_3O_4 with other cations such as Ni(II), Mn(II) and Co(II), ferrites with the general formula MFe_2O_4 can be obtained, which gives additional tools to tune the magnetic properties accordingly to the envisaged application [35, 42, 80]. A telegraphic description of the methods most used to prepare iron oxide nanoparticles is given below.

Co-precipitation

This is a widely used method to obtain iron oxide particles from mixtures of ferrous and ferric salts in aqueous basic medium [48]. The method involves the dissolution of a mixture of $FeCl_3 \cdot 6H_2O$ and $FeCl_2 \cdot 4H_2O$ in water under nitrogen atmosphere

with vigorous stirring at 70–85 °C and the subsequent addition of ammonia, leading to the formation of a dark precipitate [11, 55]. Although adaptations of this method have been employed, its simplicity and environmental friendly characteristics have made this process an elective method to prepare magnetite in aqueous medium.

Thermolysis of Precursors

The thermal decomposition of iron containing precursors in organic solvents of high boiling point temperature has been used to prepare crystalline iron oxide nanoparticles with narrow particle size distribution. Indeed, this method allows significant control of the mean size, size distribution, and provides organically protected surfaces. The reaction conditions, such as solvent, temperature, and time, are experimental parameters that can be used to adjust the final properties of the nanoparticles. Examples of precursors that have been used in this context include iron pentacarbonyl, $Fe(CO)_5$; iron(III) acetylacetonate, $Fe(C_5H_7O_2)_3$; iron(III) acetate, $Fe(CH_3CO_2)_3$, and iron(III) tri-(*N*-nitrosophenylhydroxyl-amine), i.e., $Fe(cupferron)_3$ [80, 11, 55].

Microemulsions

This method involves the use of surfactants to stabilize fine droplets of water dispersed in a nonpolar solvent. Iron salts are dissolved in water nanodroplets that are protected from the surrounding organic medium by the surfactant layer. Thus, these systems act as structured nanoreactors for synthesizing nanoparticles, proving a confined environment that limits particle nucleation and growth. A great advantage of this method is the diversity of NPs that can be obtained, both in terms of chemical composition and morphological features, by varying the chemical reactants, nature and amount of surfactant/cosurfactant, the oil phase, and the reacting conditions. For instance, $MnFe_2O_4$ nanoparticles with controllable sizes between 4 and 15 nm have been synthesized through the formation of water-in-toluene inverse micelles using sodium dodecylbenzenesulfonate (NaDBS) as surfactant [11, 55].

Hydrothermal Reactions

Hydrothermal syntheses have been used to prepare a broad range of MNPs. The reactions occur in aqueous media usually in autoclaves where the pressure can be higher than 2000 psi and the temperature can be above 200 °C. The two main routes for formation of magnetite via hydrothermal conditions involve forced hydrolysis of iron salts and thermolysis of mixed metal hydroxides. Hydrothermal reactions generally give high crystalline materials but surface capping is limited. Also, caution should be taken in the selection of the iron precursors that will be submitted to high pressure and high temperature reacting conditions. This method can be

extended to formation of other MNPs, thus $CoFe_2O_4$ nanoparticles with average size of 12 nm have been prepared by this route [11].

2.1.2 Magnetic Bionanocomposites

The preparation of magnetic bionanocomposites has involved two main approaches, the synthesis of MNPs in the presence of biopolymers (in situ) or blending of previously prepared MNPs with biopolymers (ex situ). Examples of both strategies are listed in Table 2. The synthesis in situ allows more intimate dispersion of the MNPs within the polymer matrix but control over their size and shape is limited, which in certain conditions can be crucial because nanoparticles have size and shape-dependent magnetic properties. In this situation, the biopolymer encapsulation of synthesized MNPs is an interesting alternative. Polysaccharide-based composites can be produced in the form of macroscopic networks ("bulk nanocomposites") or confined to smaller dimensions ranging the micron- to nano-metric range [18, 11]. In the latter, a variety of morphologies can be obtained depending on the preparation method employed but magnetic core–polymer shell and magnetic multi-cores homogeneously dispersed within the polymer matrix have been common structures (Fig. 2). Table 2 lists a number of magnetic sorbents used for water treatment procedures.

In situ preparation of magnetic bionanocomposites

In this strategy, magnetic bionanocomposites are prepared by promoting the synthesis of magnetic nanofillers in the biopolymer matrix. For example, polysaccharides possess functional moieties such as hydroxyl, carboxyl, and/or amine groups, which in aqueous solutions have the ability to interact with metal cations via electron rich donor atoms, which can act as nucleation sites. The cavities in the polymer network offer constrained environments that limit the growth of the in situ formed particles. The functional groups of the biopolymer present variable affinity for specific metallic ions and may determine the characteristics of the resulting inorganic phase [18, 19]. Although the one-step synthesis is relatively simpler and less time-consuming, magnetic bionanocomposites prepared by one-step procedures have been less reported. A few examples are outlined below that illustrate the usefulness of this preparative strategy.

Gum Kondagogu, an acetylated polysaccharide, was successfully used in co-precipitation of iron salts in aqueous solutions containing such biopolymer. The native gum contains various functional groups that facilitate the entrapment of MNPs within the biopolymer network by facilitating surface interactions. Transmission Electron Microscopy (TEM) images of these nanocomposites revealed spherical aggregates containing Fe_3O_4 nanoparticles with sizes ranging

Table 2 Magnetic bionanocomposites employed as sorbents in water treatment techniques

Biopolymer	MNP	Method	References
Alginate	γ-Fe_2O_3	ex situ	Rocher et al. [75]
			Ngomsik et al. [60]
			Rocher et al. [76]
			Idris et al. [40]
			Bee et al. [8]
	Fe_3O_4	ex situ	Tripathi et al. [89]
			Lee et al. [49]
	$Ni_xZn_{1-x}Fe_2O_4$	ex situ	Mahmoodi et al. [58]
	$CoFe_2O_4$	ex situ	Ai et al. [2]
Carrageenan	Fe_3O_4	ex situ	Salgueiro et al. [78]
		in situ	Mahdavinia et al. [57]
Cellulose	γ-Fe_2O_3	ex situ	Luo et al. [56]
	Fe_3O_4	ex situ	Shi et al. [81]
Carboxymethyl-β-cyclodextrin	Fe_3O_4	ex situ	Badruddoza et al. [5]
Chitosan	Fe_3O_4	ex situ	Liu et al. [52]
	γ -Fe_2O_3	in situ	Zhou et al. [105]
	γ-Fe_2O_3	ex situ	Zhou et al. [100]
		ex situ	Fan et al. [28]
			Fan et al. [27]
			Paulino et al. [63]
			Zhou et al. [102]
			Zhou et al. [103]
			Chen et al. [14]
			Zhou et al. [104]
			Liu et al. [53]
			Obeid et al. [61]
			Jiang et al. [44]
			Zhu et al. [106]
			Zhu et al. [107]
			Zhu et al. [108]
Guar gum	Fe_3O_4	ex situ	Yan et al. [97]
Gum arabic	Fe_3O_4	ex situ	Paulino et al. [64]
			Banerjee et al. [7]
Gum ghatti	Fe_3O_4	ex situ	Mittal et al. [59]
Gum kondagogu	Fe_3O_4	in situ	Saravanan et al. [79]
Sesbania gum	Fe_3O_4	ex situ	Lan et al. [46]
Humic acid	Fe_3O_4	ex situ	Peng et al. [65]
			Liu et al. [54]
			Yang et al. [98]

(continued)

Table 2 (continued)

Biopolymer	MNP	Method	References
Pectin	Fe_3O_4	ex situ	Gong et al. [33]
			Rakhshaeea et al. [70]
Poly(γ-glutamic acid)	Fe_3O_4	ex situ	Inbaraj et al. [41]
Polydopamine	Fe_3O_4	ex situ	Zhang et al. [99]
Starch	Fe_3O_4	ex situ	Pourjavadi et al. [68]

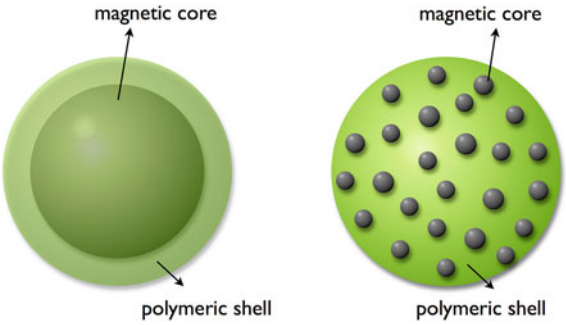

Fig. 2 Magnetic core–polymer shell (*left*) and magnetic multi-cores homogeneously dispersed in a polymer bead (*right*). Adapted from [71]

8–15 nm [79]. Magnetic iron-oxide nanoparticles have also been synthesized by in situ co-precipitation in the presence of other biopolymers such as carrageenan [57], chitosan [100, 14] and chitin/alginate [50]. Carrageenans, which are sulfated polysaccharides, were employed as stabilizers in the synthesis of magnetite nanoparticles via co-precipitation of ferric and ferrous ions and subsequent biopolymer cross-linking with K^+ ions [57], see Fig. 3. The composite beads have coarse and undulant surfaces with cubic-shaped sections, and contain Fe_3O_4 nanoparticles of sizes in the 3–7 nm range. The synthesis of magnetite nanoparticles in a chitosan matrix was prepared using W/O microemulsions containing chitosan and an Fe(II) salt [100]. The magnetic biocomposite was then treated with epichlorohydrine and grafted with ethylenediamine, in order to increase the extension of $-NH_2$ functionalization, hence increasing the adsorption capacity for anionic dyes via hydrogen bonding with protonated amine groups.

In another study, Chen et al. prepared Fe_3O_4-chitosan macroscopic beads with spherical shape of approximately 1 mm diameter by the in situ co-precipitation of Fe^{2+} and Fe^{3+} in the presence of chitosan [14]. Similarly, magnetic chitin/alginate beads were prepared in situ by promoting ionic cross-linking between the oppositely charged biopolymer chains, leading to iron oxide nanoparticles (30 nm average) uniformly dispersed and immobilized in the polymer matrix [50].

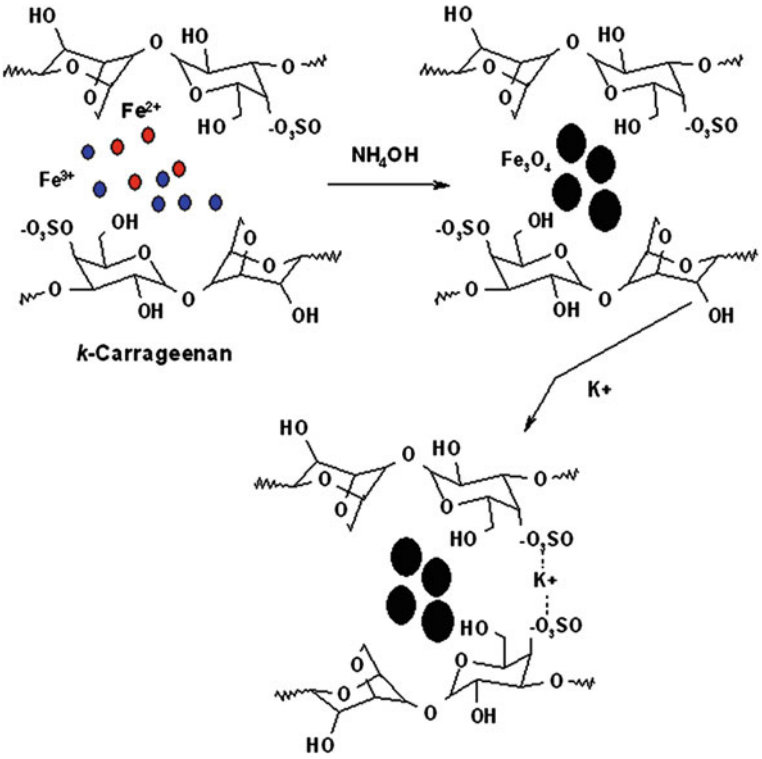

Fig. 3 Schematic representation of the preparation of magnetic κ-carrageenan beads. Reprinted with permission from [57]. Copyright 2014 Springer

Blending of magnetic nanoparticles with biopolymers

The ex situ method involves blending of MNPs with the biopolymer using a variety of methods which can be just the simple mixture of components or by inducing changes in the biopolymer, such as a cross-linking step. Typically, magnetite (Fe_3O_4) or maghemite (γ-Fe_2O_3), and more rarely a ferrite (MFe_2O_4), are obtained by synthesis methods such as those described in Sect. 2.1.1. In a second step, the MNPS are dispersed into the bulk biopolymer or its solutions, and the final composite is usually obtained by precipitation or cross-linking [71]. Surface modification of the MNPs and/or the biopolymer chains can be applied in order to ensure homogeneity of the final composite.

Alginate, a natural polysaccharide extracted from brown seaweed, was used as matrix to prepare magnetic bionanocomposites containing γ-Fe_2O_3 nanoparticles and activated carbon (AC), using Ca^{2+} ions as cross-linking agents. The resulting composite has shown spherical particles with an average diameter of 2.8 mm [76]. This route was also used to prepare macroscopic alginate beads containing cobalt ferrite and AC, which in the swollen state have an average diameter of about 2 mm. The

magnetic beads exhibited an egg-like morphology with a wrinkle and porous surface, which are characteristics that can improve the uptake of certain pollutants [2].

κ-Carrageenan coated Fe_3O_4 nanoparticles have been prepared by K^+ ions cross-linking of carrageenan chains in the presence of magnetite [78]. Acid treated and nontreated MNPs were used in order to vary the surface chemistry of the nanofillers. It was found that the bionanocomposites prepared with acid treated NPs appeared less aggregated and more homogeneously coated with the polysaccharides (Fig. 4). Acid treatment renders the surface charge of the MNP positive, thus promoting a more homogeneous dispersion in the anionic polymer. These composites were effective in the removal of methylene blue from aqueous solutions.

Chitosan-coated magnetic nanoparticles prepared by ex situ methods have been extensively reported in the literature (Table 2). Usually the preparation of magnetic chitosan composites is achieved by employing either cross-linking or precipitation methods. Zhu et al. [107] reported the preparation of crosslinked chitosan/γ-Fe_2O_3 using W/O microemulsions and glutaraldehyde as cross-linking agent. The final composite appeared as polydispersed microparticles whose average sizes range between 2 and 10 μm. Jiang et al. [44] prepared millimeter-sized γ-Fe_2O_3/chitosan

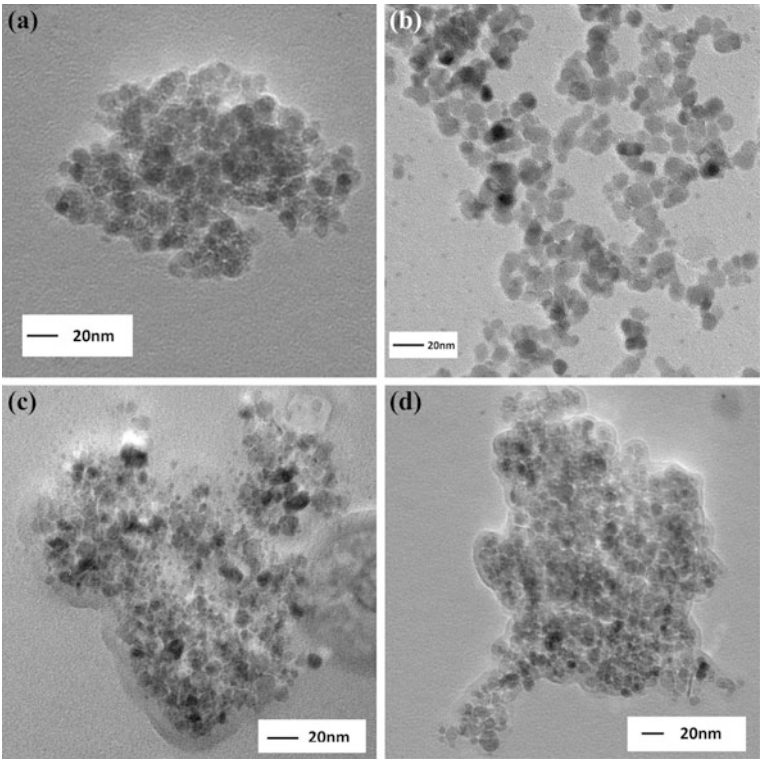

Fig. 4 TEM micrographs of **a** bare Fe_3O_4 NPs, **b** acid-treated Fe_3O_4 NPs, **c** coated Fe_3O_4 NPs and **d** coated acid-treated Fe_3O_4 NPs. Adapted with permission from [78]. Copyright 2013 Elsevier

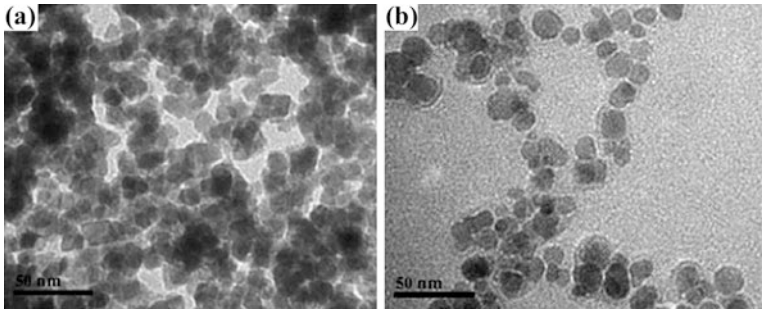

Fig. 5 TEM micrographs of **a** bare Fe_3O_4 NPs and **b** Fe_3O_4@HA NPs. Adapted with permission from [98]. Copyright 2012 American Chemical Society

beads with variable content in MNPs, which influenced the removal capacity of the composites toward Cr(VI). The composites exhibited superparamagnetic behavior and were collected from the solution by application of an external magnetic field. Magnetic chitosan biosorbents composites containing graphene oxide [27, 28] and multi-walled carbon nanotubes have been reported [108]. The incorporation of multi-walled carbon nanotubes enhanced the adsorption capacity of the composites and also improved their mechanical properties [108].

One-step coating of Fe_3O_4 nanoparticles with cellulose and chitosan was performed using ionic liquids as solvents [52]. Cellulose was used here as a blending agent for chitosan, leading to materials (average size 200 μm) with superior mechanical strength as well as to improve chemical stability in acidic medium. On the other hand, the chitosan coating prevented particle agglomeration and also provided free amine groups for coordination to aqueous heavy metal ions. Magnetite cellulose/graphene oxide composites were prepared using a co-precipitation method [81]. By loading cellulose with Fe_3O_4 NPs and GO, a rough texture at the surface of the matrix was achieved, which improved the sorption capacity of the composite in the magnetic removal of an azo dye.

Humic acid (HA) coated Fe_3O_4 nanoparticles were synthesized by co-precipitation method [98] leading to a core–shell type structure. The Fe_3O_4@HA particles appeared as spheroidal shaped with nearly uniform sizes. HA coating significantly enhanced the dispersion of Fe_3O_4@HA particles in solution compared to bare MNPs (Fig. 5).

3 Magnetism Aspects on Water Treatment Separation Technologies

3.1 General Principles of Magnetic Separation

Magnetic separation concerns overcoming a viscous flow and the associated drag force by application of a magnetic force. In the context of micro- and nano-objects,

forces associated to the mass (inertial forces) are in general negligible. In other words, such objects move within a low Reynolds number environment [69]. Thus, by removing the external (magnetic) force, MNPs will immediately stop or, in general, follow the original flow.

Magnetism can be mostly described as an interaction between dipoles, in the present case that of the magnetic particle and that of the external magnet producing a magnetic induction B. The distance between both is quite large compared to the atomic distance and therefore their interaction is solely Coulombic. This interaction has two effects: a torque that tends to align the dipoles and an attractive force that tends to bring together the dipoles.

$$\begin{aligned} \vec{F}_m &= (\vec{\mu} \cdot \nabla)\vec{B} \\ \vec{\tau} &= \vec{\mu} \times \vec{B} \end{aligned} \tag{1}$$

where μ is the moment of the dipole. It follows that magnetic separation occurs when this magnetic force is equal or larger than the drag force

$$\vec{F}_d = 6\pi\eta R\Delta\vec{v} \tag{2}$$

When the magnetic and drag forces are equal, the difference between the velocity of the nanoparticle and that of the fluid can be expressed as [62]

$$\Delta\vec{v} = \frac{R^2\Delta\chi}{9\mu_0\eta}\nabla\left(\vec{B}\cdot\vec{B}\right) \tag{3}$$

In Eq. 3, the relevant parameters are the radius (R) of the magnetic nanoparticle, the difference between the susceptibility of the nanoparticle and that of the (diamagnetic) fluid ($\Delta\chi$), and the fluid viscosity (η). Equation 3 has essentially a term associated to the magnetic properties of the system where separation occurs $(R^2\Delta\chi)/(9\mu_0\eta)$ and another term associated to the system producing the external magnetic force $\nabla\left(\vec{B}\cdot\vec{B}\right)$; both can be optimized to achieve an efficient magnetic separation. Concerning the properties of MNPs, in general, larger particles with higher magnetic susceptibility yield larger velocities. For the case of MNPs with polymer coating, Eq. 3 can be rewritten as

$$\Delta\vec{v} = \frac{R_m^3\Delta\chi}{9\mu_0\eta R_t}\nabla\left(\vec{B}\cdot\vec{B}\right) \tag{4}$$

where R_m is the radius of the magnetic nanoparticle and R_t is the total radius of the particle, such that a thicker polymer coating leads to smaller velocity difference.

Neodymium Iron Boron (NdFeB) magnets are currently the common choice to apply the external field. The $\vec{B}$ field produced by such a magnet bar is depicted in Fig. 6, showing an increase of $\vec{B}$ and its gradient when approaching the magnet pole; this increase is larger between points A and C (Fig. 6, right). More

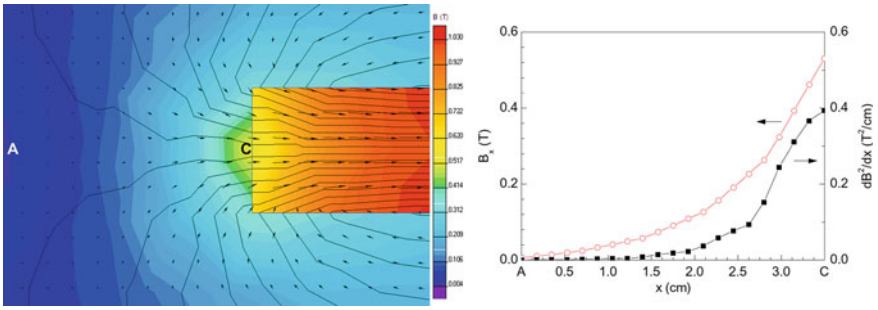

Fig. 6 *Left* color map of a typical magnetic induction created by a permanent magnet bar. *Arrows* show the direction and relative intensity of $\vec{B}$ while continuous lines represent the magnetic flux lines. Simulation performed using QuickField™ Student Edition 6.0.1.1521 by Tera Analysis Ltd using typical parameters of Neodymium Iron boron permanent magnets (1.5 × 5 cm bar, H_C = 1000 kA/m, m_r = 1.05). *Right* graph showing the dependence of the component of $\vec{B}$ along x between points A and C (B_x, open symbols, *left* scale) and the associated dependence of the term related to the magnetic force $\nabla(\vec{B}\cdot\vec{B}) = \partial B_x^2/\partial x$ (full symbols, *right* scale)

sophisticated systems using a combination of magnets yielding different field gradient profiles are also used. Another strategy is the use of micrometer sized ferromagnetic wires as a way of locally increasing the magnetic field gradient [73].

Equation 1 shows that the magnetic force is associated to the magnetic field gradient produced by a dipole.[1] As such, the MNPs will tend to move toward higher magnetic field values, usually placed at the top of the magnet (as shown in Fig. 6). In fact, the magnetic nature of a given material, diamagnetic, paramagnetic, or ferromagnetic is usually defined by the effect caused by an external magnetic field gradient, if it is repulsive, attractive, or strongly attractive, respectively. The media is usually diamagnetic and for superparamagnetic nanoparticles (to be defined below), the MNPs are attracted by the magnetic field gradient and the fluid is slightly repulsed. This is the reason why in Eq. 3 a relevant parameter is the difference between the susceptibility of the magnetic material and the media. Although magnetic forces occur only in the presence of magnetic field gradients, magnetic susceptibility χ is usually defined as the linear response of a magnetic material in the presence of a small external field H constant in space

$$M = \chi H \tag{5}$$

As stated above, in this situation torques will be developed and susceptibility quantifies the magnetization of the material that is aligned with the applied external field, i.e., it quantifies how large is the response of the stimuli to the field. A high and positive susceptibility means that a large dipolar moment appears in the direction of the field for a given field value, while a negative susceptibility means

[1] A constant magnetic field would just produce a torque.

that a dipolar moment appears in the opposite direction. Note also that we started by indistinguishably calling both the external field and the nanoparticle as 'dipoles'. In fact, they are similar in nature and magnetization of the material and intensity of the magnetic field are both a measure of the intensity of those dipoles and thus it is expectable that at magnetization and external field have equivalent units such that (volume) magnetic susceptibility is a dimensional.

3.2 Magnetic Nanoparticles for Separation Technologies

In certain situations, the atomic (ionic) magnetic moments of neighboring atoms (ions) tend to align. The origin of this alignment is in the quantum mechanical exchange integral, often introduced in the discussion of the hydrogen molecule [34], where it can be noticed that there is an energy difference between a symmetrical wave function and an antisymmetrical function, each one corresponding to a singlet spin and a triplet spin state, respectively. The singlet corresponds to an antiparallel (antiferromagnetic) coupling of spins, while the triplet corresponds to a parallel (ferromagnetic) coupling. In certain conditions, ferromagnetic and antiferromagnetic coupling leads to cooperative phenomena and properties including large magnetic moments, net magnetic moments in the absence of an external field, and hysteresis. Such phenomena occur in the case of ferromagnetic interactions and also in the case of antiferromagnetic ones, particularly when the magnitude of the coupling spins is different (as in the case of magnetite) or where the number of spins in one direction is larger than that of the opposite direction (as in the case of maghemite).

However, exchange is a short-range interaction and observation of cooperative phenomena depends on a number of factors. First, ordering can be destroyed by thermal fluctuations. Second, macroscopic ordering is favored by exchange interaction but is unfavoured by the magnetostatic energy associated with the creation of two macroscopic magnetic poles. In fact, if we take two magnetic bars into close proximity they will collapse coupling their opposite poles in order to reduce the magnetostatic energy associated to the two "isolated" magnetic poles. Third, the global energy balance has at least another important term: the anisotropy energy. This means that the energy of the system depends on the relative direction between the spins and specific directions of the material. Anisotropy energy can have different origins, being the most relevant magnetocrystalline and shape anisotropy. The magnetic state of a material will depend, in this simple description, on the balance between exchange, magnetostatic, and anisotropy energy. If anisotropy and exchange energy dominate, the system will behave as a permanent magnet. If magnetostatic energy dominates, the material will break into magnetic domains such that inside each domain the spins point in the same direction while different domains are oriented in different directions, usually forming close loops (Fig. 7a). In the case of materials forming multiple domains (such as bulk magnetite and maghemite, for instance), size changes this energy balance. Unlike magnetostatic

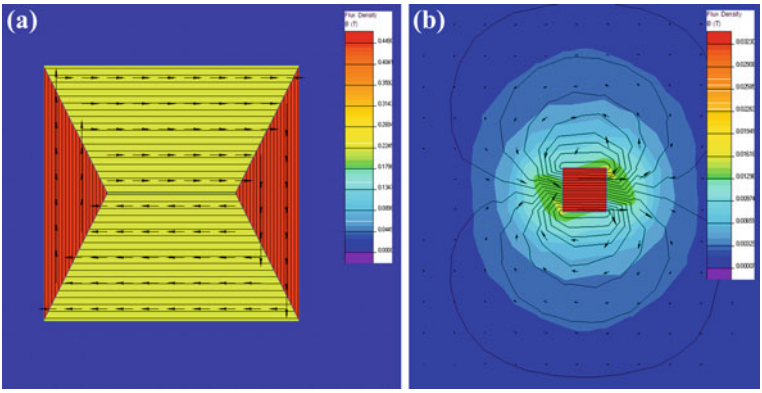

Fig. 7 **a** Color map of a typical magnetic induction created by a cubic magnetite bulk sample arbitrarily broken into four magnetic domains. Arrows show the direction and relative intensity of $\vec{B}$, while continuous lines represent the magnetic flux lines. Note that the induction outside the sample and the net magnetization of the sample are negligible. Yet, inside each domain the magnetic moments are aligned and the magnetization is not zero. **b** Similar map created by a magnetite single domain particle, where induction outside the sample is now visible and the net magnetization of the particle is not zero. Simulation performed using QuickField™ Student Edition 6.0.1.1521 by Tera Analysis Ltd using typical parameters of magnetite (H_C = 50 kA/m, m_r = 5)

energy, exchange is a short-range energy, dominating at small sizes. This means that below a given size, the system is always a single magnetic domain (Fig. 7b). This characteristic size is in the nanometric range for many materials and it is one of the key features of magnetic nanoparticles: they are intrinsically monodomains (nanodipoles). These nanoparticles are said to be superparamagnets since they are a sort of one giant classic paramagnet.

Although magnetic nanoparticles do not break into domains, the nanodipoles may have a direction fixed in space or fluctuate. The nanodipole, i.e., the magnetic moment of the nanoparticle has an intrinsic dynamic character (it fluctuates) and the fact that the direction is fixed in space or not depends on the relation between its relaxation time and the observation time window associated with a given experiment. Here, relaxation may occur between directions where anisotropy energy is minimum (the easy axis, where the dipole lies most of the time) which are separated by directions where anisotropy energy is maximum (hard directions). If the dipole is trapped in an easy axis and is not able to overcome hard axis and visit different easy directions within the observation window, the nanoparticle is said to be blocked and behaves as a nano permanent magnet. Therefore, a system composed of such nanoparticles has a nonzero net magnetization in the absence of an external field (nonzero remanence), which implies that an opposite field (the coercive field) is necessary to bring this net magnetization to zero. Otherwise, if the dipole is able to cross the anisotropy energy barrier and visit different easy axis, it is said to be unblocked, being remanence and coercivity zero. The nanoparticle is then no longer

a permanent magnet but other interesting magnetic properties arise. Many times in the literature, these are the nanoparticles termed superparamagnetic.

The fluctuation between easy axis over hard axis is usually a thermally activated process that follows an Arrhenius relation, termed Néel-Arrhenius law in this context

$$\tau_N = \tau_0 \exp\left(\frac{E_a}{k_B T}\right) \tag{6}$$

This equation gives the expected relaxation time of the nanoparticle (τ_N) for a given set of conditions: characteristic microscopic time τ_0, effective anisotropy barrier $E_a = K_{eff}V$ (proportional to the volume of the nanoparticles), and thermal energy $k_B T$. The magnetic moment of the nanoparticles is blocked (or unblocked) if τ_N is larger (or smaller) than the characteristic time of our experiment. τ_N depends exponentially on the volume and so, the design of the nanoparticles should be carefully performed concerning size, since the exponentially grows fast and we can easily pass from a situation where the nanoparticles fluctuate too fast form another where geological time scales are needed to see relaxation.

When nanoparticles which are unable to relax by the thermally activated Néel-Arrhenius mechanism are dispersed in a fluid, as usually occurs in the context of separation, another mechanism for relaxation comes into play, the Brownian relaxation. Here, the whole nanoparticle can rotate overcoming the energy associated with the viscosity of the fluid. The characteristic time for this relaxation is given as

$$\tau_B = \frac{3\eta V_H}{k_B T} \tag{7}$$

where V_H is the hydrodynamic volume of the whole nanoparticle (magnetic core plus coating). Beads composed of multi-magnetic cores wrapped by a polymer can also relax as a hole under this Brownian mechanism. Here, the dependence of the relaxation time with the volume is not so severe and a small variation in size leads to a small variation in τ_B. Particles behaving as blocked nanomagnets are usually difficult to stabilize and tend to aggregate due to the strong interparticle interactions. By contrast, unblocked nanoparticles are better dispersible yet maintaining one of their most appealing and distinctive characteristics in the context of separation: their high magnetic moment and thus high susceptibility. In unblocked superparamagnetic nanoparticles, susceptibility is given by a Curie law

$$\chi = \frac{\mu_0 N \mu^2}{3 k_B T} \tag{8}$$

where N is the number of nanoparticles per units of volume (or mass, in the case of mass susceptibility) and μ is the magnetic moment of each nanoparticle. χ is proportional to the square of μ meaning that, for instance, the susceptibility of two

nanoparticles with moment μ is less than the susceptibility of one nanoparticle made from the coalescence of these two, as long as it remains a superparamagnetic nanoparticle.

4 Application of Magnetic Bionanocomposites in Water Treatment

This section reviews the recent literature concerning application of magnetic bionanocomposites for removal of pollutants from water, thus illustrative examples will be presented for cations, dyes, and anions (Table 3). Due to the relevance of mathematical modeling of the adsorption processes involved, a brief overview of the most common models are given first. A detailed review of the several expressions for kinetics and isotherms sorption modeling can be found in the literature [66, 30].

Table 3 Magnetic bionanocomposites employed in removal of pollutants from aqueous solutions

Adsorbent	Pollutant	Optimum pH	Maximum adsorption capacity[a] (mg/g)	References
γ-Fe_2O_3—alginate—Cyanex 272	Ni(II)	5.3	0.52	Nogmsik et al. [60]
$Ni_xZn_{1-x}Fe_2O_4$-alginate	Basic Blue 9 and 41	8.0	106 and 25	Mahmoodi [58]
	Basic Red 18		56	
γ-Fe_2O_3—alginate beads containing activated carbon	Methylene Blue		5.9×10^{-2} mmol/g	Rocher et al. [76]
	Methyl Orange		2×10^{-3} mmol/g	
γ-Fe_2O_3—alginate	Pb(II)	7.0	50	Idris et al. [40]
Fe_3O_4—alginate-agarose	U(VI)	5.0	120.5	Tripathi et al. [89]
Fe_3O_4—alginate-chitosan beads	La(III)	2.8	97.1	Wu et al. [94]
Fe_3O_4—cellulose-graphene oxide	Methylene Blue		70.03	Shi et al. [81]
Fe_3O_4—Gum ghatti	Rhodamine B	7.0	654.87	Mittal and Mishra [59]
Iron oxide—Gum kondagogu (modified)	Cd(II), Cu(II), Pb (II), Ni(II), Zn (II), Hg(II)	5.0 ± 0.1	106.8, 85.9, 56.6, 49.0, 37.0, 35.0	Saravanan et al. [79]
Fe_3O_4—Humic acid	Eu(III)	8.5	6.95×10^{-5} mol/g	Yang et al. [98]
Fe_3O_4—κ-carrageenan	Methylene Blue	9	185.3	Salgueiro et al. [78]

(continued)

Table 3 (continued)

Adsorbent	Pollutant	Optimum pH	Maximum adsorption capacity[a] (mg/g)	References
Fe_3O_4—chitosan-graphene oxide composite	Methylene Blue	10.0	180.83	Fan et al. [27]
Iron oxide—chitosan composite	UO_2(II), Th(IV)		666.67, 312.50	Hritcu et al. [38]
Fe_3O_4—chitosan microspheres	Hg(II), Cu(II), Ni(II)	5.0	60.06, 42.93, 12.15	Zhou et al. [102]
γ-Fe_2O_3—chitosan	Cr(VI)	5.0	106.5	Jiang et al. [44]
γ-Fe_2O_3/SiO_2—chitosan	Methyl Orange	2.95	34.29	Zhu et al. [109]
Fe_3O_4—thiourea-chitosan imprinted Ag^+	Ag(I)	5.0	5.29	Fan et al. [26]

[a]Experimental or estimated values from applied models

4.1 Modeling the Adsorption Process

The adsorption of pollutants onto bionanocomposites is a complex process that can involve different mechanisms, including chemisorption, metal complexation, ion-exchange, precipitation, and physical adsorption [23]. The chemical nature of the pollutants and bionanocomposites, the removal conditions (e.g. pH, temperature, and ionic strength) and structural features (e.g. porosity) play an important role in determining the mechanisms involved that, in turn, will affect the adsorption rate. Moreover, the rate of the overall adsorption process might also be limited by the steps that anticipate the adsorption of the solute to the sorbent's surface, including the transport of solute from the bulk of the solution to the surroundings of the sorbent, the diffusion of the solute across the liquid film surrounding the sorbent (external diffusion), and the diffusion of the solute in the liquid within sorbent pores (intraparticle diffusion) [66]. The establishment of appropriate adsorption equilibrium correlation is indispensable for assessing the performance of a sorbent aiming at quantitative comparison of the adsorption capacity of different sorbents. Additionally, predicting the rate at which the pollutants removal takes place is crucial for effective design of adsorption systems. In this perspective, attempts have been made to describe the kinetics and the equilibrium sorption conditions using mathematical models. Table 4 lists the most representative isotherm and kinetic equations used for describing the adsorption of water pollutants.

The Langmuir equation [47] derives from an isotherm model commonly applied to describe the equilibrium of sorption on magnetic bionanocomposites [60, 40, 81, 102, 14, 104, 59, 98, 94, 26]. This empirical model assumes monolayer adsorption at a finite number of sites that are identical and equivalent, without any interaction between molecules adsorbed on adjacent sites. According to this model once a molecule occupies a site, no further adsorption can take place. The Freundlich isotherm [31] is an empirical model that describes the nonideal and reversible

Table 4 Isotherm and kinetic equations commonly used for describing the adsorption process of water pollutants

Isotherm models		Kinetic models	
Langmuir	$q_e = \frac{q_m K_L C_e}{1+K_L C_e}$	Pseudo-first order	$q_t = q_e(1 - e^{-k_1 t})$
Freundlich	$q_e = K_F C_e^{1/n_F}$	Pseudo-second order	$q_t = \frac{k_2 q_e^2 t}{1+k_2 q_e t}$
Sips	$q_e = q_m \frac{K_s C_e^{n_S}}{1+K_s C_e^{n_S}}$	Elovich	$q_t = \frac{1}{B}\ln(1 + ABt)$
Redlich-Peterson	$q_e = K_{RP} \frac{C_e}{1+\alpha_{RP} C_e^{\beta}}$	Intraparticle Diffusion	$q_t = C + k_P t^{1/2}$
Tempkin	$q_e = \frac{RT}{b_t}\ln(a_t C_e)$		

q_t is the adsorption capacity, i.e., the amount of solute adsorbed at time t; q_e is the adsorption capacity at equilibrium; q_m is the maximum adsorption capacity estimated by the model; C_e is the concentration of the solute at equilibrium; K_L is the Langmuir equilibrium constant; K_F and n_F are Freundlich constants and β is a parameter in the range 0–1; K_S and n_S are Sips constants; K_{RP} and α_{RP} are Redlich-Peterson constants; R is the gas constant; T is the absolute temperature; b_t is a constant related to the heat of adsorption and a_t is the Tempkin isotherm constant; k_1 is the pseudo-first order rate constant; k_2 is the pseudo-second order rate constant; A and B are Elovich constants; k_p is the intraparticle rate constant and C is the intercept

adsorption and accounts for the formation of multilayers with nonuniform distribution of adsorption heat and affinities over heterogeneous surfaces. Because the equation is exponential, usually it provides good fitting only in low to moderate concentration ranges of the sorbate. The Sips isotherm [82] combines the Langmuir and Freundlich expressions and it is usually applied for describing heterogeneous adsorption. At low adsorbate concentration it reduces to Freundlich isotherm while at high concentration it predicts the monolayer adsorption characteristic of the Langmuir isotherm. Similar to the Sips equation, the Redlich-Peterson isotherm [72] is an empirical model that also compromises the features of the Langmuir and Freundlich equations. It is a versatile equation than can be applied either in homogeneous or heterogeneous adsorption, over a wide sorbate concentration range. This isotherm equation described very well the adsorption of Pb(II), Cd(II) Cu(II) and Cr(VI) ions onto magnetic chitosan-based biocomposites [63, 21]. The Tempkin isotherm [85] assumes that adsorption heat of molecules in the layer decreases linearly with coverage. This is explained due to the sorbent–sorbate interactions and the distribution of binding energies in the adsorption is uniform. This isotherm fitted well the removal of the dye Basic Blue 9 using magnetic alginate composites [58].

The pseudo-first and the pseudo-second order equations are expressions commonly used for describing sorption kinetics, although they cannot be considered sorption kinetic models in their physical sense since they are used to describe the kinetics of other phenomena as well. The pseudo-first-order equation has been widely used to predict the adsorption of solutes from liquid solutions in systems near equilibrium and in systems with a time-independent solute concentration or linear behavior in equilibrium adsorption isotherms [83]. In contrast with the previous model, the pseudo-second-order kinetic equation predicts the behavior over the

whole range of adsorption [37]. The Elovich model [77] neglects the rate of simultaneously occurring desorption and therefore its applicability if often restricted to the initial times of the sorption process [66]. This model was suitable for describing the kinetic behavior of the adsorption of the reactive dye red 222 in chitosan-based materials [95]. In the same work the authors analyzed the kinetic data found in the literature for several biopolymer-based adsorption systems and found that the Elovich model fits well the adsorption kinetics of those systems with mildly rising tendency. The intraparticle diffusion model was proposed by Weber and Morris [93] who found that in many adsorption systems, the adsorption capacity varies almost proportionally with $t^{1/2}$ rather than with contact time t. This model assumes that the intraparticle–diffusion is the rate-limiting step of the solute uptake.

4.2 Removal of Metal Ions

Hazardous metal ions are commonly found in natural and wastewaters as dissolved contaminants. Some of these cations have been considered priority pollutants, such as Hg(II), thus requiring effective processes for their removal from water. A range of bionanocomposites has been investigated as effective sorbents for metal ions removal; here only those with ability for magnetic separation will be considered.

Alginate magnetic beads have shown great efficiency in the uptake of Pb(II) ions from aqueous solutions [40]. The adsorption equilibrium was achieved in less than 3 h in the pH range 6–10, with maximum adsorption observed at pH 7. The results fitted well to the Langmuir adsorption model with maximum adsorption capacity about 50 mg/g. Also, alginate-agarose magnetite composites have been applied in the removal of U(VI) from aqueous medium. The maximum uranium adsorption (97 ± 2 %) was observed in the pH range of 4.5–5.5. The thermodynamic parameters suggested passive endothermic adsorption behavior [89]. The performance of magnetic alginate-chitosan beads for the adsorption of lanthanum ions from aqueous solutions was evaluated. The materials showed selective high adsorption for lanthanum among other coexisting ions, such as Pb(II), Cd(II), Co (II), Ni(II) and Cu(II), with a maximum uptake of 97.1 mg/g. The adsorption data correlated well with the Langmuir isotherm model, while the kinetic data fit well the pseudo- second-order model [94]. Ngomsik et al. [60] evaluated the adsorption of Ni(II) from aqueous solutions using magnetic alginate microcapsules containing Cyanex 27 extractant. A two-stage kinetics behavior was observed with 70 % of maximum sorption capacity achieved within 8 h. An increase on Ni(II) removal was observed by increasing the pH, with a maximum uptake capacity of 0.42 mmol/g at pH 8. The adsorption isotherm (pH about 5.3) was obtained for a range of Ni(II) initial concentrations; the experimental data fitted the Langmuir model and the maximum adsorption capacity was reported as 0.52 mmol/g.

Humic acid (HA) coated Fe_3O_4 nanoparticles were investigated as sorbents for removal of various aqueous cations such as Hg(II), Pb(II), Cd(II), and Cu(II) [54].

The sorption of these ions reached equilibrium in less than 15 min, and agrees well with the Langmuir adsorption model with maximum adsorption capacities ranging from 45 to 100 mg/g. The composite was able to remove over 99 % of Hg(II) and Pb(II), and over 95 % of Cu(II) and Cd(II) in natural and tap water at optimized pH. More recently, Yang et al. [98] investigated the removal of Eu(III) ions from aqueous solutions by Fe_3O_4@HA composites. A fast sorption kinetics was observed, equilibrium reached in less than 30 min, with high sorption capacity attributed to abundant surface sites for coordination provided by the HA macromolecules. The composites were able to remove ~99 % of Eu(III) in aqueous solution at pH 8.5. The sorption isotherm agreed well with the Langmuir model, having a maximum sorption capacity of 6.95×10^{-5} mol/g.

The adsorption ability of Gum kondagogu modified Fe_3O_4 nanoparticles was investigated in the removal of a variety of metal ions [30]. The removal efficiencies of the different cations followed the order: Cd(II) > Cu(II) > Pb(II) > Ni(II) > Zn (II) > Hg(II), while for the overall desorption (%) of these ions the following series was established: Pb(II) > Cu(II) > Cd(II) > Hg(II) > Ni(II) > Zn(II), at pH = 5.0 ± 0.1 and temperature of 30.0 ± 1.0 °C. A maximum of 106.8 mg/g and a minimum of 35.07 mg/g adsorption capacities were observed, respectively, for Cd (II) and Hg(II), using the Langmuir isotherm model.

Sebasnia gum magnetic nanocomposites were used as adsorbents to remove Cd (II), Cu(II), and Pd(II). Consecutive sorption–desorption cycles were repeated thrice to establish the reusability of the adsorbent. The composite shows desorption efficiencies after the regeneration process above 91.19 % for Cu (II), 96.69 % for Cd (II), and 87.61 % for Pb (II) ions [46].

Chitosan and derivative composites have been widely used as sorbents to remove heavy metal ions from aqueous solutions. Figure 8 illustrates the overall process of adsorption, desorption and recycling in using magnetite cellulose–chitosan hydrogels for the removal of metal ions [52]. These studies have shown that the hydrogels had scarce affinity to Mn(II), Zn(II), and Ni(II), but exhibited high affinity to Cu(II), Fe(II), and Pb(II), with corresponding equilibrium adsorption capacities (mg/g) of, respectively, 44.7 ± 5, 94.1 ± 7 and 28.1 ± 3 of the adsorbent (dried weight).

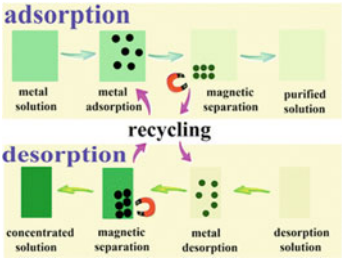

Fig. 8 Overall process of metal adsorption, desorption and recycling of magnetite cellulose-chitosan hydrogels. Reprinted with permission from [52]. Copyright 2012 Royal Society of Chemistry

Zhou et al. [104] prepared chitosan-coated maghemite nanoparticles modified with α-ketoglutaric acid and evaluated the ability to remove Cu(II) ions from the aqueous solution. Equilibrium studies have shown that Cu(II) adsorption data follow the Langmuir model, and the maximum adsorption capacity for Cu(II) ions was estimated as 96.15 mg/g. Also, magnetite chitosan hydrogels, graft-copolymerized with methylenebisacrylamide, and poly(acrylic acid) were employed in studies on the adsorption kinetics of Pb (II), Cd(II), and Cu(II) in aqueous solution [63]. The best experimental parameters for removal of metal ions have been observed at pH 4.5–5.5, initial metal concentration of 300 mg/dm^3 and 100 mg of dried hydrogel mass as sorbent. Isotherm models of Langmuir, Freundlich, and Redlich–Peterson were applied and revealed that the adsorption efficiency decreased with the presence of magnetite. The removal of Hg(II), Cu(II), and Ni(II) ions from aqueous solutions mediated by thiourea modified magnetite chitosan microspheres was investigated [104]. The adsorption kinetics followed the mechanism of pseudo-second-order equation for all systems studied, evidencing chemical sorption as the rate-limiting step of adsorption mechanism and not involving mass transfer in solution. The best interpretation for the equilibrium data was given by a Langmuir isotherm, and the maximum adsorption capacities were 625.2, 66.7 and 15.3 mg/g for Hg(II), Cu(II), and Ni(II) ions, respectively. Fan et al. [26] prepared magnetite thiourea-chitosan composites using Ag(I) as an imprinted ion and were able to show that this resin is strongly selective for the adsorption of Ag(I) over Cd(II), Zn(II), Pb(II), and Cu(II). The equilibrium adsorption was achieved within 50 min and the maximum adsorption capacity was 4.93 mmol/g observed at pH 5 and temperature 30 °C. The kinetic data, obtained at optimum pH 5, could be fitted with a pseudo-second order equation. Furthermore, the adsorption process was well described by Langmuir adsorption. In another study, monodisperse chitosan-coated Fe_3O_4 nanoparticles were used as adsorbents for recovery of Au(III) ions from aqueous solutions. Au(III) ions could be fast and efficiently adsorbed, and the adsorption capacity increased with decrease in pH due to protonation of the amino groups of chitosan. The adsorption data obeyed the Langmuir equation with a maximum adsorption capacity of 59.52 mg/g (1210 mg/g based on weight of chitosan) and a Langmuir adsorption equilibrium constant of 0.066 mg^{-1}. From the studies on the adsorption kinetics and thermodynamics of Au(III) ions, it was found that the adsorption process obeyed the pseudo-second-order kinetic model [12]. Magnetic chitosan composites were used as sorbents for removal of radioactive species from aqueous medium [14, 38, 101]. Magnetic chitosan composite particles exhibited high adsorption capacity for both UO_2(II) (666.67 mg/g) and Th(IV) (312.50 mg/g) and the authors conclude that the OH and –NH_2 groups were involved in this process [38]. In another study, Chen et al. [14] evaluated the capacity of Fe_3O_4-chitosan beads to remove Sr(II) ions from aqueous solutions. The adsorption equilibrium was reached at 6 h and the maximum adsorption capacity was calculated to be 11.58 mg/g using the Langmuir isotherm.

4.3 Removal of Dyes

In addition to metal ions, magnetic bionanocomposites have also been applied in the removal of dyes from aqueous solutions. These organic pollutants can be present in the effluents of industries of a number of products that include textiles, papers, plastics, among others. The discharge of dyes in water supplies is a matter of concern due to their harmful impact on the environment. Most of these compounds are potentially harmful to aquatic life and several dyes and their degradation products exhibit toxicity and potential mutagenic and carcinogenic effects [90].

Magnetic alginate composites have been investigated as sorbents for magnetic removal of dyes from aqueous solutions [76, 58, 2]. Ai et al. [2] reported the preparation of AC-$CoFe_2O_4$-alginate composites for effective removal of methylene blue (MB) from aqueous solutions. The kinetic studies revealed that the adsorption process followed the pseudo-first-order kinetic model. In addition, the adsorption equilibrium was well described by the Langmuir and Freundlich models. In another study, Mahmodi [58] investigated the ability of a nickel-zinc ferrite-alginate composite to remove dyes from both single and binary systems. Basic Blue 9 (BB9), Basic Blue 41 (BB41) and Basic Red 18 (BR18) were selected as model pollutants. The data obtained in single systems showed that the experimental data correlated reasonably well by the Tempkin (BB9) and Langmuir (BB41 and BR18) isotherm models. The data also indicated that the adsorption kinetics of dyes on the adsorbents followed the intraparticle diffusion model at different adsorbent dosages.

Rocher et al. [76] combined the adsorption properties of AC and the magnetic properties of γ-Fe_2O_3 NPs in an alginate matrix to produce a magnetic sorbent. The sorbent ability toward cationic MB and anionic methyl orange (MO) dyes was then evaluated. The adsorption kinetics reached equilibrium after 180 min, 50 % of the amount of MB was adsorbed in 10 min, while for MO this percentage of adsorption was achieved at 17 min contact time. Also, cellulose beads entrapping γ-Fe_2O_3 NPs and AC have been investigated for removal of such dyes from aqueous medium. Although the beads effectively adsorbed both dyes, these systems have shown higher adsorption capacity for MO than for MB. This reveals that the negatively charged MO was easier to bind with the beads through hydrogen bonding and electrostatic interaction. So the system could adsorb more strongly the negatively charge organic dyes (MO) than positively charged MB, indicating a selective adsorption behavior [56].

Mittal and Mishra [59] incorporated Fe_3O_4 NPs in a matrix of gum ghatti cross-linked with poly(acrylic acid-co-acrylamide) for removal of rhodamine B (RhB) from aqueous solutions. The adsorption at pH 7 of RhB onto the nanocomposite was endothermic and involved an increase in entropy. The process followed the Langmuir adsorption model and a maximum adsorption capacity of 654.87 mg/g was reported. The pseudo-second-order kinetic model described better the adsorption process than other kinetic models with high correlation coefficients.

Furthermore, the adsorbent showed good reproducibility and reusability for successive three cycles.

κ-Carrageenan coated Fe_3O_4 nanoparticles were tested as adsorbents for the magnetically assisted removal of MB from aqueous solutions [78]. The dye uptake was found to vary with solution pH and was higher in alkaline conditions. Both pseudo-first-order and pseudo-second-order equations predicted well the kinetics with the maximum adsorption achieved very fast, within 5 min. Interestingly, in this case MB adsorption has shown an unusual Z-type isotherm, which was interpreted by the generation of new adsorbing sites with increasing MB initial concentration. Under the experimental conditions used (23 °C, pH 9) the materials displayed MB adsorption capacity of 185.3 mg/g.

A chitosan-coated magnetite composite containing alizarin red (AR) as imprinted molecules was prepared and used to remove AR from aqueous solutions [26]. A maximum adsorption capacity of 40.12 mg/g was observed at pH 3 and temperature 30 °C. Equilibrium adsorption was achieved within 50 min. The kinetic data, obtained at the optimum pH 3, could be fitted with a pseudo-second-order equation. Furthermore, the adsorption process could be well described by Langmuir adsorption isotherms. The same group reported the preparation of similar magnetic chitosan composites but containing GO for the removal of MB [27]. The MB maximum adsorption capacity was 180.83 mg/g and the adsorption process was well fitted by the pseudo-second-order kinetic model. The incorporation of carbon nanostructures in magnetic chitosan-based sorbents was also explored by wrapping multiwalled carbon nanotubes and γ-Fe_2O_3 nanoparticles for the purpose of removal of MO [108].

Zhu et al. [109] prepared a γ-Fe_2O_3-SiO_2-chitosan composite and investigated the adsorption performance of this composite toward MO dissolved in water. The adsorption kinetics was found to follow the pseudo-second-order kinetic model, and intraparticle diffusion was related to adsorption, but not as a sole rate-controlling step. The equilibrium adsorption data were well described by the Freundlich isotherm model. The same group investigated the adsorptive potential of chitosan-kaolin-γ-Fe_2O_3 [106] and γ-Fe_2O_3-crosslinked chitosan [107] composites for removal of MO. Kalkan and co-workers [45] prepared magnetite nanoparticles coated with chitosan and applied it for removal of the reactive textile dye Reactive Yellow 145. The dye adsorption occurs according to the Langmuir model in the temperature range of 25–45 °C with a maximum adsorption capacity of 47.63 mg/g at 25 °C.

Magnetite NPs were synthesized onto guar gum-grafted carbon nanotubes to prepare a magnetic composite for adsorption of red (MR) and methylene blue (MB) from aqueous solutions [97]. The grafting of guar gum onto the carbon nanotubes (CNTs) enhances their hydrophilicity, thus improving their dispersion in aqueous solutions. The adsorption behavior of the composite for MB and NR could be described well by the pseudo second-order model. The adsorption isotherm experiments revealed that the adsorption data fitted Langmuir isotherm model, and the maximum adsorption of MB and NR reached 61.92 and 89.85 mg/g.

Multiwall carbon nanotubes-starch-Fe_3O_4 composite was used as an adsorbent for removing anionic dye methyl orange (MO) and cationic dye methylene blue (MB) from aqueous solutions [13]. The use of hydrophilic starch improved the dispersion of the composite in aqueous solutions and increased the number of surface sites available for dyes adsorption. The adsorption behavior was well described by the pseudo second-order model and the maximum adsorption capacities at equilibrium were 135.6 mg/g for MO and 93.7 mg/g for MB.

Debrassi et al. [22] prepared magnetic *N*-benzyl-O-carboxymethylchitosan nanoparticles and applied these nanosorbents on removal of three cationic dyes: MB, crystal violet (CV), and malachite green (MG). A pseudo-second-order equation was the best-fitted equation to characterize the adsorption process for the three dyes, among four kinetic models applied. The Langmuir–Freundlich equation was the best isotherm model, and maximum adsorption capacities of 223.58, 248.42 and 144.79 mg/g were reported for MB, CV, and MG, respectively.

4.4 Removal of Anions

The major sources of water contamination by large amounts of certain anions are domestic and agriculture activities. The intensive use of fertilizers in agriculture and forestry sectors has strong impact on contamination of natural waters by certain anions [3]. There have been attempts to use magnetic biocomposites for removal of such anions from contaminated water. For example, Lee and Kim [49] developed magnetic alginate-layered double hydroxide composites for phosphate removal. The results have shown that the magnetic composites were effective in the removal of phosphate and equilibrium was reached at 24 h. The maximum phosphate sorption capacity was determined to be 39.1 mgP/g. In addition, phosphate removal was not much sensitive to the initial solution pH (between 4.1 and 10.2).

Chitosan beads containing nanosized γ-Fe_2O_3 were prepared for Cr(VI) removal in the form of dissolved dichromate ($Cr_2O_7^{2-}$) and the effect of pH and coexisting ions on the magnetic removal was investigated [44]. The sorbent showed excellent performance in removal of $Cr_2O_7^{2-}$ from water with a maximum sorption capacity

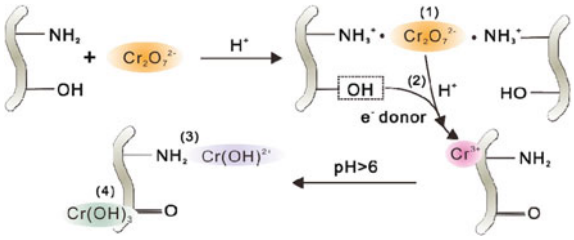

Fig. 9 Scheme for the mechanism proposed in the interaction of Cr(VI) with γ-Fe_2O_3—chitosan beads. Reprinted with permission from [44]. Copyright 2013 American Chemical Society

of 106.5 mg/g in the concentration range 0–200 ppm. The determination of the thermodynamic parameters indicates the spontaneous and exothermic nature of the sorption process. The γ-Fe_2O_3- chitosan bionanocomposite beads kept their performance after six cycles regeneration. The sorption of Cr(VI) on the beads has been described by a series of processes as illustrated in Fig. 9. Hence, dichromate species were first adsorbed on the beads surface via electrostatic attraction, occurring reduction to Cr(III) by the –OH groups of chitosan and coordination of the Cr(III) ions by the amine groups on the bead surfaces. In these processes there is consumption of hydrogen ions, which result in increase of the solution pH.

In some regions, arsenic can be present as a dangerous contaminant of water in the form of arsenate (AsO_4^{3-}) and/or arsenite (AsO_3^{3-}). The toxicity and mobility of arsenic are affected by its oxidation state, with arsenite as more toxic and mobile than arsenate in aqueous environments. Arsenate removal by calcium alginate-encapsulated magnetic sorbents has been investigated [51]. Fourier transform infrared spectroscopy (FTIR) and X-ray photoelectron spectroscopy (XPS) were used to assess the interaction between arsenic species and available sites of the sorbent. These studies indicate that surface oxygen of the magnetite and hydroxyl groups of the calcium alginate composite play an important role in the sorption of arsenate ions. Based on the XPS analysis it has been proposed that arsenate is reduced to arsenite after adsorption onto the sorbent.

Water-soluble molybdate anions represent a threat to the environment for concentrations exceeding 5 ppm. Therefore, the development of materials for treatment of water with high levels of such anions is an important issue. Elwakeel et al. [25] prepared two chemically modified chitosan resins incorporating magnetite NPs for removal of Mo oxoanions from aqueous solutions via anion exchange. Chitosan resins bearing both amine and quaternary ammonium chloride moieties (R2) displayed higher uptake capacity than the analog with only amine (R1) groups.

5 Conclusions and Future Perspectives

The application of magnetic bionanocomposites as sorbents for magnetic separation in water treatment has emerged as an interesting alternative to conventional sorbents. These materials offer clear advantages due to their potential bio- and eco-compatibility, tuned magnetic behavior, and affinity for a variety of pollutants, aiming at development of magnetic separation technologies of interest for water treatment units. Implementation of surface chemical modifications to adjust the affinity/specificity toward distinct pollutants has been demonstrated in various contexts, but more research is required, namely evaluation in real samples of diverse chemical composition and from different sources. These sorbents offer the clear advantage of magnetic separation by applying an external magnetic field in confined spaces. This aspect has important consequences in terms of waste storage, or recycling and reuse of sorbents, but on the other hand implies further developments on magnetic separation technology.

Acknowledgments F.L. Sousa acknowledges FCT (Fundação para a Ciência e a Tecnologia) for SFRH/BPD/71033/2010 grant. A.L. Daniel-da-Silva and N.J.O. Silva acknowledge FCT for funding from Ciência 2008 program and IF2013 contract, respectively. The authors thank funding by FEDER through COMPETE- Programa Operacional Factores de Competitividade and national funding from FCT in the frame of the project PTDC/CTM-NAN/120668/2010 and FCOMP-01-0124-FEDER-037271 (Ref. Pest-C/CTM/LA0011/2013).

References

1. Ahmaruzzaman M (2011) Industrial wastes as low-cost potential adsorbents for the treatment of wastewater laden with heavy metals. Adv Colloid Interface Sci 166:36–59
2. Ai L, Li M, Li L (2011) Adsorption of methylene blue from aqueous solution with activated carbon/cobalt ferrite/alginate composite beads: kinetics, osotherms, and thermodynamics. J Chem Eng Data 56:3475–3483
3. Ali I (2012) New generation adsorbents for water treatment. Chem Rev 112:5073–5091
4. Babel S, Kurniawan TA (2003) Low-cost adsorbents for heavy metals uptake from contaminated water: a review. J Hazard Mater 97:219–243
5. Badruddoza AZM, Tay ASH, Tan PY, Hidajat K, Uddin MS (2011) Carboxymethyl-β-cyclodextrin conjugated magnetic nanoparticles as nano-adsorbents for removal of copper ions: Synthesis and adsorption studies. J Hazard Mater 185:1177–1186
6. Bailey SE, Olin TJ, Bricka RM, Adrian DD (1999) A review of potentially low-cost sorbents for heavy metals. Water Res 33:2469–2479
7. Banerjee SS, Chen D-H (2007) Fast removal of copper ions by gum arabic modified magnetic nano-adsorbent. J Hazard Mater 147:792–799
8. Bee A, Talbot D, Abramson S, Dupuis V (2011) Magnetic alginate beads for Pb(II) ions removal from wastewater. J Colloid Interface Sci 362:486–593
9. Bhattacharyya KG, Gupta SS (2008) Adsorption of a few heavy metals on natural and modified kaolinite and montmorillonite: A review. Adv Colloid Interface Sci 140:114–131
10. Blackburn RS (2004) Natural polysaccharides and their interactions with dye molecules: applications in effluent treatment. Environ Sci Technol 38:4905–4909
11. Carlos L, Einschlag FSG, González MC, Mártire DO (2013) Waste water – treatment technologies and recent analytical developments. Intech – Open Access Publisher
12. Chang Y-C, Chen D-H (2006) Recovery of gold(III) ions by a chitosan coated magnetic nano-adsorbent. Gold Bulletin 39:98–102
13. Chang PR, Zheng P, Liu B, Anderson DP, Yu J, Ma X (2011) Characterization of magnetic soluble starch-functionalized carbon nanotubes and its application for the adsorption of the dyes. J Hazard Mater 186:2144–2150
14. Chen Y, Wang J (2012) Removal of radionuclide Sr^{2+} ions from aqueous solution using synthesized magnetic chitosan beads. Nucl Eng Des 242:445–451
15. Crini G (2005) Recent developments in polysaccharide-based materials used as adsorbents in wastewater treatment. Prog Polym Sci 30:38–70
16. Crini G (2006) Non-conventional low-cost adsorbents for dye removal: A review. Bioresour Technol 97:1061–1085
17. Daniel-da-Silva AL, Carvalho RS, Trindade T (2013) Magnetic hydrogel nanocomposites and composite nanoparticles – a review of recent patented works. Recent Pat Nanotechnol 7:153–166
18. Daniel-da-Silva AL, Silva NJO, Gil AM, Trindade T (2011) Nano-composite particles for bio-applications: Materials and bio-interfaces. Pan Stanford Publishing Pte. Ltd., Singapore
19. Daniel-da-Silva AL, Trindade T (2011) Advances in nanocomposite technology. Intech – Open Access Publisher

20. Dave SR, Gao X (2009) Monodisperse magnetic nanoparticles for biodetection, imaging, and drug delivery: a versatile and evolving technology. Wires Nanomed Nanobi 1:583–609
21. Debnath S, Maity A, Pillay K (2014) Magnetic chitosan–GO nanocomposite: Synthesis, characterization and batch adsorber design for Cr(VI) removal. J Environ Chem Eng 2:963–973
22. Debrassi A, Corrêa AF, Baccarin T, Nedelko N, Slawska-Waniewsk A, Sobczak K, Dłuzwskib P, Greneche J-M, Rodrigues CA (2012) Removal of cationic dyes from aqueous solutions using N-benzyl-O-carboxymethylchitosan magnetic nanoparticles. Chem Eng J 183:284–293
23. Demirbas A (2008) Heavy metal adsorption onto agro-based waste materials: A review. J Hazard Mater 157:220–229
24. Dias AMGC, Hussain A, Marcos AS, Roque ACA (2011) A biotechnological perspective on the application of iron oxide magnetic colloids modified with polysaccharides. Biotechnol Adv 29:142–155
25. Elwakeel KZ, Atia AA, Donia AM (2009) Removal of Mo(VI) as oxoanions fromaqueous solutions using chemically modified magnetic chitosan resins. Hydrometallurgy 97:21–28
26. Fan L, Luo C, Lv Z, Lu F, Qui H (2011) Removal of Ag^+ from water environment using a novel magnetic thiourea-chitosan imprinted Ag^+. J Hazard Mater 194:193–201
27. Fan L, Luo C, Sun M, Li X, Lu F, Qiu H (2012) Preparation of novel magnetic chitosan/graphene oxide composite as effective adsorbents toward methylene blue. Bioresour Technol 114:703–706
28. Fan L, Luo C, Sun M, Li X, Qiu H (2013) Highly selective adsorption of lead ions by water-dispersible magnetic chitosan/graphene oxide composites. Colloids Surf B 103:523–529
29. Fan L, Zhang Y, Li X, Luo C, Lu F, Qiu H (2012) Removal of alizarin red from water environment using magnetic chitosan with Alizarin Red as imprinted molecules. Colloids Surf B 91:250–257
30. Foo KY, Hameed BH (2010) Insights into the modeling of adsorption isotherm systems. Chem Eng J 156:2–10
31. Freundlich HMF (1906) Over the adsorption in solution. J Phys Chem 57:385–471
32. Girginova PI, Daniel-da-Silva AL, Lopes CB, Figueira P, Otero M, Amaral VS, Pereira E, Trindade T (2010) Silica coated magnetite particles for magnetic removal of Hg2+ from water. J Colloid Interface Sci 345:234–240
33. Gong J-L, Wang X-Y, Zeng G-M, Chen L, Deng J-H, Zhang X-R, Niu Q-Y (2012) Copper (II) removal by pectin–iron oxide magnetic nanocomposite adsorbent. Chem Eng J 185–186:100–107
34. Goodenough JB (1963) Magnetism and the chemical bond. John Wiley and Sons, New York
35. Guglielmo CD, López DR, Lapuente JD, Mallafre JML, Suàrez MB (2010) Embryotoxicity of cobalt ferrite and gold nanoparticles: a first in vitro approach. Reprod Toxicol 30:271–276
36. Gupta AK, Gupta M (2005) Synthesis and surface engineering of iron oxide nanoparticles for biomedical applications. Biomater 26:3995–4021
37. Ho YS, McKay G (1999) Pseudo-second order model for sorption processes. Process Biochem 34:451–465
38. Hritcu D, Humelnicu D, Dodi G, Popa MI (2012) Magnetic chitosan composite particles: Evaluation of thorium and uranyl ion adsorption from aqueous solutions. Carbohydr Polym 87:1185–1191
39. Hu J, Lo IMC, Chen G (2004) Removal of Cr(VI) by magnetite. Water Sci Technol 50:139–146
40. Idris A, Ismail NSM, Hassan N, Misran E, Ngomsik A-F (2012) Synthesis of magnetic alginate beads based on maghemite nanoparticles for Pb(II) removal in aqueous solution. J Ind Eng Chem 18:1582–1589
41. Inbaraj BS, Chen BH (2011) Dye adsorption characteristics of magnetite nanoparticles coated with a biopolymer poly(γ-glutamic acid). Bioresour Technol 102:8868–8876

42. Indira TK, Lakshmi PK (2010) Magnetic nanoparticles–a review. Int Pharm Sci Nanotech 3:1035–1042
43. Jeong U, Teng X, Wang Y, Yang H, Xia Y (2007) Superparamagnetic colloids: controlled synthesis and niche applications. Adv Mater 19:33–60
44. Jiang Y-J, Yu X-Y, Luo T, Jia Y, Liu J-H, Huang X-J (2013) γ-Fe_2O_3 Nanoparticles encapsulated millimeter-sized magnetic chitosan beads for removal of Cr(VI) from water: Thermodynamics, kinetics, regeneration, and uptake mechanisms. J Chem Eng Data 58:3142–3149
45. Kalkan NA, Aksoy S, Aksoy EA, Hasirci N (2012) Adsorption of reactive yellow 145 onto chitosan coated magnetite nanoparticles. J Appl Polym Sci 124:576–584
46. Lan S, Leng Z, Guo N, Wu X, Gan S (2014) Sesbania gum-based magnetic carbonaceous nanocomposites: Facile fabrication and adsorption behavior. Colloids Surf A 446:163–171
47. Langmuir I (1918) The adsorption of gases on plane surfaces of glass, mica and platinum. J Am Chem Soc 40:1361–1406
48. Laurent S, Forge D, Port M, Roch A, Robic C, Elst LV, Muller RN (2008) Magnetic iron oxide nanoparticles: synthesis, stabilization, vectorization, physicochemical characterizations, and biological applications. Chem Rev 108:2064–2110
49. Lee C-G, Kim S-B (2013) Magnetic alginate-layered double hydroxide composites for phosphate removal. Environ Technol 34:2749–2756
50. Li G, Du Y, Tao Y, Deng H, Luo X, Yang J (2010) Iron(II) cross-linked chitin-based gel beads: Preparation, magnetic property and adsorption of methyl orange. Carbohydr Polym 82:706–713
51. Lim S-F, Zheng Y-M, Zou S-W, Chen JP (2009) Uptake of arsenate by an alginate-encapsulated magnetic sorbent: Process performance and characterization of adsorption chemistry. J Colloid Interface Sci 333:33–39
52. Liu Z, Wang H, Liu C, Jiang Y, Yu G, Mu X, Wang X (2012) Magnetic cellulose–chitosan hydrogels prepared from ionic liquids as reusable adsorbent for removal of heavy metal ions. Chem Commun 48:7350–7352
53. Liu B, Wang D, Li H, Xu Y, Zhang L (2011) As(III) removal from aqueous solution using α-Fe_2O_3 impregnated chitosan beads with As(III) as imprinted ions. Desalination 272:286–1292
54. Liu J-F, Zhao Z-S, Jiang G-B (2008) Coating Fe_3O_4 magnetic nanoparticles with humic acid for high efficient removal of heavy metals in water. Environ Sci Technol 42:6949–6954
55. Lu A-H, Salabas EL, Schüth F (2007) Magnetic nanoparticles: synthesis, protection, functionalization, and application. Angew Chem Int Ed 46:1222–1244
56. Luo X, Zhang L (2009) High effective adsorption of organic dyes on magnetic cellulose beads entrapping activated carbon. J Hazard Mater 171:340–347
57. Mahdavinia GR, Iravani S, Zoroufi S, Hosseinzadeh H (2014) Magnetic and K+-cross-linked kappa-carrageenan nanocomposite beads and adsorption of crystal violet. Iran Polym J 23:335–344
58. Mahmoodi NM (2013) Magnetic ferrite nanoparticle–alginate composite: Synthesis, characterization and binary system dye removal. J Taiwan Inst Chem Eng 44:322–330
59. Mittal H, Mishra SB (2014) Gum ghatti and Fe_3O_4 magnetic nanoparticles based nanocomposites for the effective adsorption of rhodamine B. Carbohydr Polym 101:1255–1264
60. Ngomsik A-F, Bee A, Siaugue J-M, Cabuil V, Cote G (2006) Nickel adsorption by magnetic alginate microcapsules containing an extractant. Water Res 420:1848–1856
61. Obeid L, Bée A, Talbot D, Jaafar SB, Dupuis V, Abramson S, Cabuil V, Welschbillig M (2013) Chitosan/maghemite composite: A magsorbent for the adsorption of methyl orange. J Colloid Interface Sci 410:52–58
62. Pankhurst QA, Connolly J, Jones SK, Dobson J (2003) Applications of magnetic nanoparticles in biomedicine. J Phys D: Appl Phys 36:R167–R181
63. Paulino AT, Belfiore LA, Kubota LT, Muniz EC, Almeida VC, Tambourgi EB (2011) Effect of magnetite on the adsorption behavior of Pb(II), Cd(II), and Cu(II) in chitosan-based hydrogels. Desalination 275:187–196

64. Paulino AT, Guilherme MR, Mattoso LHC, Tambourgi EB (2010) Smart hydrogels based on modified gum arabic as a potential device for magnetic biomaterial. Macromol Chem Phys 211:1196–1205
65. Peng L, Qin P, Lei M, Zeng Q, Song H, Yang J, Shao J, Liao B, Gu J (2012) Modifying Fe_3O_4 nanoparticles with humic acid for removal of Rhodamine B in water. J Hazard Mater 209–210:193–198
66. Plazinski W, Rudzinski W, Plazinska A (2009) Theoretical models of sorption kinetics including a surface reaction mechanism: A review. Adv Colloid Interface Sci 152:2–13
67. Polyak B, Friedman G (2009) Magnetic targeting for site-specific drug delivery: applications and clinical potential. Expert Opin Drug Del 6:53–70
68. Pourjavadi A, Hosseini SH, Seidi F, Soleyman R (2013) Magnetic removal of crystal violet from aqueous solutions using polysaccharide-based magnetic nanocomposite hydrogels. Polym Int 62:1038–1044
69. Purcell EM (1977) Life at low reynolds number. Am J Phys 45:3–11
70. Rakhshaeea R, Panahandeh M (2011) Stabilization of a magnetic nano-adsorbent by extracted pectin to remove methylene blue from aqueous solution: A comparative studying between two kinds of cross-likened pectin. J Hazard Mater 189:158–166
71. Reddy DHK, Lee SM (2013) Application of magnetic chitosan composites for the removal of toxic metal and dyes from aqueous solutions. Adv Colloid Interface Sci 201–202:68–93
72. Redlich O, Peterson DL (1959) A useful adsorption isotherm. J Phys Chem 63:1024–1026
73. Ritter JA, Ebner AD, Daniel KD, Stewart KL (2004) Application of high gradient magnetic separation principles to magnetic drug targeting. J Magn Magn Mater 280:184–201
74. Rivera-Utrilla J, Sánchez-Polo M, Gómez-Serrano V, Alvarez PM, Alvim-Ferraz M CM, Dias JM (2011) Activated carbon modifications to enhance its water treatment applications. An overview. J Hazard Mater 187:1–23
75. Rocher V, Bee A, Siaugue J-M, Cabuil V (2010) Dye removal from aqueous solution by magnetic alginate beads crosslinked with epichlorohydrin. J Hazard Mater 178:434–439
76. Rocher V, Siaugue J-M, Cabuil V, Bee A (2008) Removal of organic dyes by magnetic alginate beads. Water Res 42:1290–1298
77. Roginsky S, Zeldovich Y (1934) Acta Physicochim USSR 1:554
78. Salgueiro AM, Daniel-da-Silva AL, Girão AV, Pinheiro PC, Trindade T (2013) Unusual dye adsorption behavior of κ-carrageenan coated superparamagnetic nanoparticles. Chem Eng J 229:276–284
79. Saravanan P, Vinod VTP, Sreedhar B, Sashidhar RB (2012) Gum kondagogu modified magnetic nano-adsorbent: An efficient protocol for removal of various toxic metal ions. Mater Sci Eng C 32:581–586
80. Sharifi I, Shokrollahi H, Amiri S (2012) Ferrite-based magnetic nanofluids used in hyperthermia applications. J Magn Magn Mater 324:903–915
81. Shi H, Li W, Zhong L, Xu C (2014) Methylene blue adsorption from aqueous solution by magnetic cellulose/graphene oxide composite: Equilibrium, kinetics, and thermodynamics. Ind Eng Chem Res 53:1108–1118
82. Sips R (1948) Combined form of Langmuir and Freundlich equations. J Chem Phys 16:490–495
83. Soto ML, Moure A, Dominguez H, Parajó JC (2001) Recovery, concentration and purification of phenolic compounds by adsorption: A review. J Food Eng 105:1–27
84. Tang SCN, Lo IMC (2013) Magnetic nanoparticles: Essential factors for sustainable environmental applications. Water Res 47:2613–2632
85. Tempkin MJ, Pyzhev V (1940) Recent modification to Langmiur isotherms. Acta Physiochim USSR 12:217–222
86. Thakur VK, Thakur MK (2014) Processing and characterization of natural cellulose fibers/thermoset polymer composites. Carbohydrate Polymers 109:102–117

87. Thakur VK, Thakur MK, Raghavan P, Kessler MR (2014) Progress in green polymer composites from lignin for multifunctional applications: A review. ACS Sustain Chem Eng 2:1072–1092
88. Tong J, Chen L (2013) Review: Preparation and application of magnetic chitosan derivatives in separation processes. Anal Lett 46:2635–2656
89. Tripathi A, Melo JS, D'Souza SF (2013) Uranium (VI) recovery from aqueous medium using novel floating macroporous alginate-agarose-magnetite cryobeads. J Hazard Mat 246–247:87–95
90. Umbuzeiro GA, Freeman HS, Warren SH, de Oliveira DP, Terao Y, Watanabe T, Claxton LD (2005) The contribution of azo dyes to the mutagenic activity of the Cristais River. Chemosphere 60:55–64
91. Vettorazzi G (1979) International regulatory aspects for pesticide chemicals. CRC Press Inc.: Boca Raton, Florida
92. Wang Ngah WS, Teong LC, Hanafiah MAKM (2011) Adsorption of dyes and heavy metal ions by chitosan composites: A review. Carbohydrate Polymers 83:1446–1456
93. Weber Jr WJ, Morris JC (1963) Kinetics of adsorption on carbon from solution. J Sanit Eng Div Am Soc Civ Engrs 89:31–59
94. Wu D, Zhang L, Wang L, Zhu B, Fan L (2011) Adsorption of lanthanum by magnetic alginate-chitosan gel beads. J Chem Technol Biotechnol 86:345–352
95. Wu F-C, Tseng R-L, Juang R-S (2009) Characteristics of Elovich equation used for the analysis of adsorption kinetics in dye-chitosan systems. Chem Eng J 150:366–373
96. Xu P, Zeng GM, Huang DL, Feng CL, Hu S, Zhao MH, Lai C, Wei Z, Huang C, Xie GX, Liu ZF (2012) Use of iron oxide nanomaterials in wastewater treatment: A review. Sci Total Environ 424:1–10
97. Yan L, Chang PR, Zheng P, Ma X (2012) Characterization of magnetic guar gum-grafted carbon nanotubes and the adsorption of the dyes. Carbohydr Polym 87:1919–1924
98. Yang S, Zong P, Ren X, Wang Q, Wang X (2012) Rapid and highly efficient preconcentration of Eu(III) by core–shell structured Fe_3O_4@humic acid magnetic nanoparticles. ACS Appl Mater Interfaces 4:6891–6900
99. Zhang S, Zhang Y, Bi G, Liu J, Wang Z, Xu Q, Xu H, Li X (2014) Mussel-inspired polydopamine biopolymer decorated with magnetic nanoparticles for multiple pollutants removal. J Hazard Mater 270:27–34
100. Zhou L, Jin J, Liu Z, Liang X, Shang C (2011) Adsorption of acid dyes from aqueous solutions by the ethylenediamine-modified magnetic chitosan nanoparticles. J Hazard Mater 185:1045–1052
101. Zhou L, Shang C, Liu Z, Huang G, Adesina AA (2012) Selective adsorption of uranium(VI) from aqueous solutions using the ion-imprinted magnetic chitosan resins. J Colloid Interface Sci 366:165–172
102. Zhou L, Wang Y, Liu Z, Huang Q (2009) Characteristics of equilibrium, kinetics studies for adsorption of Hg(II), Cu(II), and Ni(II) ions by thiourea-modified magnetic chitosan microspheres. J Hazard Mater 161:995–1002
103. Zhou Y, Fu S, Zhang L, Zhang H, Levit MV (2014b) Use of carboxylated cellulose nanofibrils-filled magnetic chitosan hydrogel beads as adsorbents for Pb(II). Carbohydr Polym 101:75–82
104. Zhou Y-T, Nie H-L, Branford-White C, He Z-Y, Zhu L-M (2009) Removal of Cu^{2+} from aqueous solution by chitosan-coated magnetic nanoparticles modified with α-ketoglutaric acid. J Colloid Interface Sci 330:29–37
105. Zhou Z, Lin S, Yue T, Lee T-C (2014a) Adsorption of food dyes from aqueous solution by glutaraldehyde cross-linked magnetic chitosan nanoparticles. J Food Eng 126:133–141
106. Zhu H-Y, Jiang R, Xiao L (2010) Adsorption of an anionic azo dye by chitosan/kaolin/γ-Fe_2O_3 composites. Appl Clay Sci 48:522–526
107. Zhu H-Y, Jiang R, Xiao L, Li W (2010) A novel magnetically separable γ-Fe_2O_3/crosslinked chitosan adsorbent: Preparation, characterization and adsorption application for removal of hazardous azo dye. J Hazard Mater 179:251–257

108. Zhu H-Y, Jiang R, Xiao L, Zeng GM (2010) Preparation, characterization, adsorption kinetics and thermodynamics of novel magnetic chitosan enwrapping nanosized γ-Fe_2O_3 and multi-walled carbon nanotubes with enhanced adsorption properties for methyl orange. Bioresour Technol 101:5063–5069
109. Zhu HY, Jiang R, Fu Y-Q, Jiang J-H, Xiao L, Zeng G-M (2011) Preparation, characterization and dye adsorption properties of γ-Fe_2O_3/SiO_2/chitosan composite. Appl Surf Sci 258:1337–1344